Model independent measurement of form factors in the decay $D^+ \to K^-\pi^+e^+\nu_e$

M. R. Shepherd,[1] D. Besson,[2] T. K. Pedlar,[3] D. Cronin-Hennessy,[4] K. Y. Gao,[4] D. T. Gong,[4] J. Hietala,[4] Y. Kubota,[4] T. Klein,[4] B. W. Lang,[4] R. Poling,[4] A. W. Scott,[4] A. Smith,[4] P. Zweber,[4] S. Dobbs,[5] Z. Metreveli,[5] K. K. Seth,[5] A. Tomaradze,[5] J. Ernst,[6] H. Severini,[7] S. A. Dytman,[8] W. Love,[8] V. Savinov,[8] O. Aquines,[9] Z. Li,[9] A. Lopez,[9] S. Mehrabyan,[9] H. Mendez,[9] J. Ramirez,[9] G. S. Huang,[10] D. H. Miller,[10] V. Pavlunin,[10] B. Sanghi,[10] I. P. J. Shipsey,[10] B. Xin,[10] G. S. Adams,[11] M. Anderson,[11] J. P. Cummings,[11] I. Danko,[11] J. Napolitano,[11] Q. He,[12] J. Insler,[12] H. Muramatsu,[12] C. S. Park,[12] E. H. Thorndike,[12] F. Yang,[12] T. E. Coan,[13] Y. S. Gao,[13] F. Liu,[13] M. Artuso,[14] S. Blusk,[14] J. Butt,[14] J. Li,[14] N. Menaa,[14] R. Mountain,[14] S. Nisar,[14] K. Randrianarivony,[14] R. Redjimi,[14] R. Sia,[14] T. Skwarnicki,[14] S. Stone,[14] J. C. Wang,[14] K. Zhang,[14] S. E. Csorna,[15] G. Bonvicini,[16] D. Cinabro,[16] M. Dubrovin,[16] A. Lincoln,[16] D. M. Asner,[17] K. W. Edwards,[17] R. A. Briere,[18] I. Brock,[18] J. Chen,[18] T. Ferguson,[18] G. Tatishvili,[18] H. Vogel,[18] M. E. Watkins,[18] J. L. Rosner,[19] N. E. Adam,[20] J. P. Alexander,[20] K. Berkelman,[20] D. G. Cassel,[20] J. E. Duboscq,[20] K. M. Ecklund,[20] R. Ehrlich,[20] L. Fields,[20] R. S. Galik,[20] L. Gibbons,[20] R. Gray,[20] S. W. Gray,[20] D. L. Hartill,[20] B. K. Heltsley,[20] D. Hertz,[20] C. D. Jones,[20] J. Kandaswamy,[20] D. L. Kreinick,[20] V. E. Kuznetsov,[20] H. Mahlke-Krüger,[20] T. O. Meyer,[20] P. U. E. Onyisi,[20] J. R. Patterson,[20] D. Peterson,[20] J. Pivarski,[20] D. Riley,[20] A. Ryd,[20] A. J. Sadoff,[20] H. Schwarthoff,[20] X. Shi,[20] S. Stroiney,[20] W. M. Sun,[20] T. Wilksen,[20] M. Weinberger,[20] S. B. Athar,[21] R. Patel,[21] V. Potlia,[21] J. Yelton,[21] P. Rubin,[22] C. Cawlfield,[23] B. I. Eisenstein,[23] I. Karliner,[23] D. Kim,[23] N. Lowrey,[23] P. Naik,[23] C. Sedlack,[23] M. Selen,[23] E. J. White,[23] and J. Wiss[23]

(CLEO Collaboration)

[1]*Indiana University, Bloomington, Indiana 47405, USA*
[2]*University of Kansas, Lawrence, Kansas 66045, USA*
[3]*Luther College, Decorah, Iowa 52101, USA*
[4]*University of Minnesota, Minneapolis, Minnesota 55455, USA*
[5]*Northwestern University, Evanston, Illinois 60208, USA*
[6]*State University of New York at Albany, Albany, New York 12222, USA*
[7]*University of Oklahoma, Norman, Oklahoma 73019, USA*
[8]*University of Pittsburgh, Pittsburgh, Pennsylvania 15260, USA*
[9]*University of Puerto Rico, Mayaguez, Puerto Rico 00681*
[10]*Purdue University, West Lafayette, Indiana 47907, USA*
[11]*Rensselaer Polytechnic Institute, Troy, New York 12180, USA*
[12]*University of Rochester, Rochester, New York 14627, USA*
[13]*Southern Methodist University, Dallas, Texas 75275, USA*
[14]*Syracuse University, Syracuse, New York 13244, USA*
[15]*Vanderbilt University, Nashville, Tennessee 37235, USA*
[16]*Wayne State University, Detroit, Michigan 48202, USA*
[17]*Carleton University, Ottawa, Ontario, Canada K1S 5B6*
[18]*Carnegie Mellon University, Pittsburgh, Pennsylvania 15213, USA*
[19]*Enrico Fermi Institute, University of Chicago, Chicago, Illinois 60637, USA*
[20]*Cornell University, Ithaca, New York 14853, USA*
[21]*University of Florida, Gainesville, Florida 32611, USA*
[22]*George Mason University, Fairfax, Virginia 22030, USA*
[23]*University of Illinois, Urbana-Champaign, Illinois 61801, USA*
(Received 1 June 2006; published 8 September 2006)

We present model independent measurements of the helicity basis form factors in the decay $D^+ \to K^-\pi^+e^+\nu_e$ obtained from about 2 800 decays reconstructed from a 281 pb^{-1} data sample collected at the $\psi(3770)$ center-of-mass energy with the CLEO-c detector. We confirm the existence of a previously observed spin-zero $K^-\pi^+$ component interfering with the $\bar{K}^{*0}$ amplitude. We see no evidence for additional d- or f-wave contributions.

DOI: 10.1103/PhysRevD.74.052001 PACS numbers: 13.20.Fc, 12.38.Qk, 14.40.Lb

I. INTRODUCTION

Exclusive semileptonic decays are excellent probes of charm decay dynamics since strong interaction effects only enter through the current coupling the parent D meson with the final state hadronic system [1]. This current is generally expressed in terms of form factors that depend on q^2, the squared invariant mass of the virtual W^+ materializing as a positron-neutrino pair. The specific q^2 dependence is an ansatz in most of the models, although the ultimate goal is to derive both normalization and q^2 dependence from first principles. Various theoretical approaches have been pursued to study semileptonic form factors, such as quark models [2], QCD sum rules [3], lattice QCD [4], and the parametrization of the form factor q^2 dependence based on effective poles [5] constrained by heavy quark and soft collinear effective theories. Measurements of both the branching fraction [6] and the q^2 dependence of the form factors [7] have been made for the $D^+ \to \bar{K}^{*0}\ell^+\nu_\ell$ decays using specific parametrizations [7]. Recently, Ref. [8] reported a first observation of an additional component besides the dominant $D^+ \to \bar{K}^{*0}\ell^+\nu_\ell$ in the $D^+ \to K^-\pi^+\ell^+\nu_\ell$ decay process. In the additional component, K^- and π^+ are in a relative s-wave, which has revealed an interesting connection between semileptonic decays and light quark physics. According to Ref. [9], $2.4 \pm 0.7\%$ of the decays in the mass range $0.8\ \mathrm{GeV}/c^2 < m_{K\pi} < 1.0\ \mathrm{GeV}/c^2$ are due to this s-wave component, where $m_{K\pi}$ is the $K^-\pi^+$ mass.

Using a technique developed by FOCUS [10], we present nonparametric measurements of the q^2 dependence of the helicity basis form factors that describe an amplitude for the $K^-\pi^+$ system to be in any one of its possible angular momentum states. This is done by projecting out the helicity form factors directly from data without the use of fitting functions. Our results will allow theorists to directly compare their models with the data free from parametrization. We also confirm the existence of the s-wave component, study its form factor for the first time, and limit the strength of possible d- and f-wave contributions.

There are several good reasons to perform this analysis using the CLEO-c data: The q^2 resolution in CLEO-c is an order of magnitude better than in FOCUS. In addition, the $D^+ \to \bar{K}^{*0}e^+\nu_e$ process is simpler than $D^+ \to \bar{K}^{*0}\mu^+\nu_\mu$, since there is a negligible probability for the much less massive e^+ to be left-handed which eliminates one of the form factors. The additional form factor describing the left-handed ℓ^+ coupling has an angular distribution so similar to H_0 in Eq. (1) that it degrades the measurement of H_0 by a factor of 3.

The amplitude $\mathcal{M}$ for the semileptonic decay $D^+ \to K^-\pi^+e^+\nu_e$ is described by five kinematic quantities: q^2, $m_{K\pi}$, the angle between the π and the D direction in the $K^-\pi^+$ rest frame (θ_V), the angle between the ν_e and the D direction in the $e^+\nu_e$ rest frame (θ_ℓ), and the acoplanarity angle between the two decay planes (χ). Following Ref. [9], we can express the matrix element for the decay $D^+ \to K^-\pi^+e^+\nu_e$ in the vicinity of the $\bar{K}^{*0}$ mass in terms of the three helicity amplitudes ($H_+(q^2)$, $H_-(q^2)$, and $H_0(q^2)$) describing the pseudoscalar to vector hadronic current and one form factor ($h_0(q^2)$) describing a broad s-wave resonance. The dominant terms in the differential width $|\mathcal{M}|^2$, integrated over the angle χ can be expressed as:

$$\int |\mathcal{M}|^2 d\chi \propto G_F^2 |V_{cs}|^2 (q^2 - m_\ell^2)[((1+\cos\theta_\ell)\sin\theta_V)^2 |H_+(q^2)|^2 |BW|^2 + ((1-\cos\theta_\ell)\sin\theta_V)^2 |H_-(q^2)|^2 |BW|^2 + (2\sin\theta_\ell\cos\theta_V)^2 |H_0(q^2)|^2 |BW|^2 + 8\sin^2\theta_\ell\cos\theta_V H_0(q^2) h_0(q^2)\,\mathrm{Re}\{\mathcal{A}e^{-i\delta}BW\} + \mathcal{O}(\mathcal{A}^2)]. \quad (1)$$

The second to last term in Eq. (1) represents the interference between the s-wave $K^-\pi^+$ and the $\bar{K}^{*0}$ amplitude, where $\mathcal{A}$ and δ represent the amplitude and the phase of the s-wave, respectively. Since the s-wave amplitude could be observed only through interference with the $\bar{K}^{*0}$, FOCUS was sensitive to the s-wave amplitude only in the vicinity of the $\bar{K}^{*0}$ pole. They modeled the s-wave contribution as a constant complex amplitude, even though a variation of the amplitude with respect to $m_{K\pi}$ is possible. In this paper, we assume the $\mathcal{A}$ and δ values obtained in Ref. [9] in the study of the $h_0(q^2)H_0(q^2)$ interference term. The $\bar{K}^{*0}$ amplitude in Eq. (1) is represented as a Breit-Wigner of the form:

$$BW = \frac{\sqrt{m_0\Gamma}(\frac{P^*}{P_0^*})}{m_{K\pi}^2 - m_0^2 + im_0\Gamma(\frac{P^*}{P_0^*})^3},$$

where P^* is the kaon momentum in the $K^-\pi^+$ rest frame and P_0^* is the kaon momentum in this frame at the resonant mass m_0. The χ integration significantly simplifies the intensity by eliminating all interference terms between different helicity states of the virtual W^+ with relatively little loss in form factor information. We have dropped the term which is second order in the small, s-wave amplitude $\mathcal{A}$.

The three helicity basis form factors for the $D^+ \to \bar{K}^{*0} e^+ \nu_e$ component are generally written [11] as linear combinations of vector ($V(q^2)$) and axial-vector ($A_{1,2}(q^2)$) form factors according to Eq. (2):

$$H_{\pm}(q^2) = (M_D + m_{K\pi})A_1(q^2) \mp 2\frac{M_D \tilde{K}}{M_D + m_{K\pi}} V(q^2) \quad \text{and}$$
$$H_0(q^2) = \frac{1}{2m_{K\pi}\sqrt{q^2}}\left[(M_D^2 - m_{K\pi}^2 - q^2)(M_D + m_{K\pi})A_1(q^2) - 4\frac{M_D^2 \tilde{K}^2}{M_D + m_{K\pi}} A_2(q^2)\right], \tag{2}$$

where M_D is the mass of the D^+ and $\tilde{K}$ is the momentum of the $K^-\pi^+$ system in the rest frame of the D^+.

In this paper, we use a *projective weighting* technique [10] to disentangle and directly measure the q^2 dependence of these helicity basis form factors free from parametrization. We provide information on the form factor products $H_{\pm}^2(q^2)$, $H_0^2(q^2)$, and $h_0(q^2)H_0(q^2)$ in bins of q^2 by projecting out the associated angular factors given by Eq. (1).

II. EXPERIMENTAL AND ANALYSIS DETAILS

The CLEO-c detector [12] consists of a six-layer, low-mass, stereo-wire drift chamber, a 47-layer central drift chamber, a ring-imaging Čerenkov detector (RICH), and a cesium iodide electromagnetic calorimeter inside a superconducting solenoidal magnet providing a 1.0 T magnetic field. The tracking chambers and the electromagnetic calorimeter cover 93% of the full solid angle. The solid angle coverage for the RICH detector is 80% of 4π. Identification of the charged pions and kaons is based on measurements of specific ionization (dE/dx) in the main drift chamber and RICH information. In positron identification, in addition to dE/dx and RICH information, the ratio of energy deposited in the electromagnetic calorimeter to the measured track momentum (E/p) is used.

In this paper, we use 281 pb^{-1} of data taken at the $\psi(3770)$ center-of-mass energy with the CLEO-c detector at the Cornell Electron Storage Ring (CESR), which corresponds to a sample of 0.8×10^6 D^+D^- pair events [13]. Monte Carlo (MC) events are generated by EVTGEN [14] and the detector is simulated using a GEANT-based [15] program. Simulation of final state radiation is handled by PHOTOS [16]. Throughout this paper charge-conjugate modes are implied.

We select events where a $D^+ \to K^-\pi^+e^+\nu_e$ candidate is produced against a fully reconstructed tagging D^-. The tagging D^- decays into one of the following six decay modes: $D^- \to K_S^0\pi^-$, $D^- \to K^+\pi^-\pi^-$, $D^- \to K_S^0\pi^-\pi^0$, $D^- \to K^+\pi^-\pi^-\pi^0$, $D^- \to K_S^0\pi^-\pi^-\pi^+$, and $D^- \to K^-K^+\pi^-$. Multiple D^- candidates per event are allowed. More details on selecting the tagging D^- candidates as well as identifying π^0 and K_S^0 candidates are described in Ref. [13].

The following selection cuts represent our *nominal selection* criteria. The semileptonic D^+ reconstruction starts by requiring three well-measured tracks not coming from the tagging D^- decay in the event. Charged kaons and pions are required to have momenta of at least 50 MeV/c and are identified using dE/dx and RICH information. Positron candidates are required to have momenta of at least 200 MeV/c, satisfy $|\cos\theta| < 0.9$, where θ is the angle between the positron and the beam line, and pass a requirement on a likelihood variable that combines E/p, dE/dx, and RICH information. We obtain 2 838 $D^+ \to K^-\pi^+e^+\nu_e$ events. Finally, we require 0.8 GeV/$c^2 \le m_{K\pi} \le 1.0$ GeV/c^2 and select 2 472 events. The $m_{K\pi}$ distribution for these $D^+ \to K^-\pi^+e^+\nu_e$ candidates is shown in Fig. 1. In our analysis, the only particle not reconstructed is the neutrino of the $D^+ \to K^-\pi^+e^+\nu_e$ decay. The neutrino four-momentum can be reconstructed from the energy-momentum balance in the beam-beam center-of-mass frame. We assign the neutrino the missing energy ($E_{\rm miss}$) which is the difference between the beam energy ($E_{\rm beam}$) and the sum of the energies of the charged semileptonic daughters. The neutrino momentum is obtained from direction of the missing momentum ($\hat{p}_{\rm miss} = \vec{p}_{\rm miss}/|\vec{p}_{\rm miss}|$) defined as:

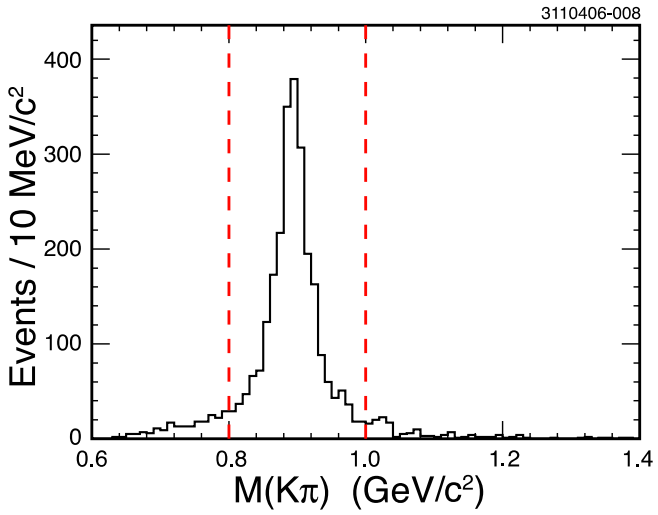

FIG. 1 (color online). The $m_{K\pi}$ distribution for events satisfying our *nominal* $D^+ \to K^-\pi^+e^+\nu_e$ selection requirements. Over the full displayed mass range, there are 2 838 events satisfying our nominal $D^+ \to K^-\pi^+e^+\nu_e$ selection. For this analysis, we use a restricted mass range 0.8–1.0 GeV/c^2 (shown by the vertical dashed lines). In this restricted region, there are 2 472 events.

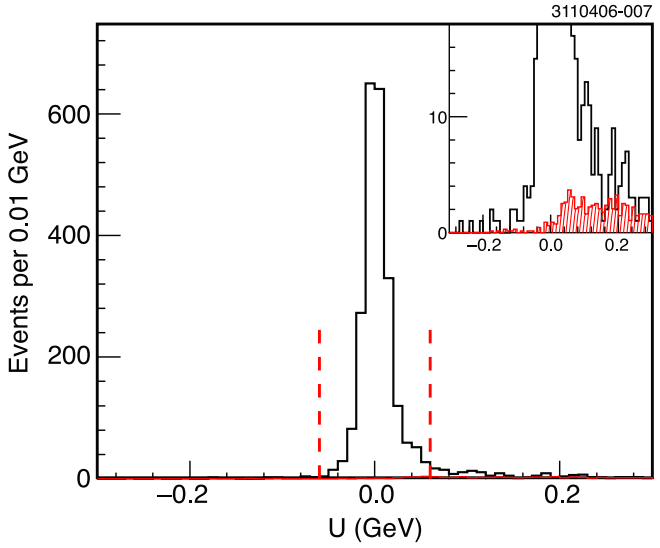

FIG. 2 (color online). The observed energy imbalance U distribution for $D^+ \to K^-\pi^+e^+\nu_e$ events satisfying our *nominal* selection. We show the boundaries for the additional $|U| < 0.06$ GeV requirement used for the *tighter* selection. The inset is the same distribution on a finer scale where the background contribution estimated from a Monte Carlo sample is more apparent as a hashed histogram.

$$\vec{p}_{\,\mathrm{miss}} = -\sqrt{E_{\mathrm{beam}}^2 - m_D^2}\,\hat{p}_{D^-} - \vec{p}_{K^-} - \vec{p}_{\pi^+} - \vec{p}_{e^+}. \quad (3)$$

In Eq. (3), $\hat{p}_{D^-}$ is the measured direction of the tagging D^-, $\vec{p}$ is the measured momentum of the indicated particle, and m_D is the known mass of the D^- [17]. The magnitude of the neutrino momentum is set to E_{miss}.

We will compare the *nominal* selection to a *tighter* selection where we add two further restrictions: $0.846\ \mathrm{GeV}/c^2 \le m_{K\pi} \le 0.946\ \mathrm{GeV}/c^2$ and $|U| < 0.06$ GeV, where $U \equiv E_{\mathrm{miss}} - c|\vec{p}_{\mathrm{miss}}|$. Figure 2 shows the U distribution for the nominally selected sample with the background contribution. The background shape in Fig. 2 is obtained using a charm MC set which consists of generic $D\bar{D}$ events. We estimate a background level of 3.6% for the nominal selection and 0.4% for the tighter selection. We have checked the MC background simulation with a sample of wrong sign events where we reconstructed the semileptonic candidates with electrons instead of positrons and obtained consistent results between the data and the MC samples.

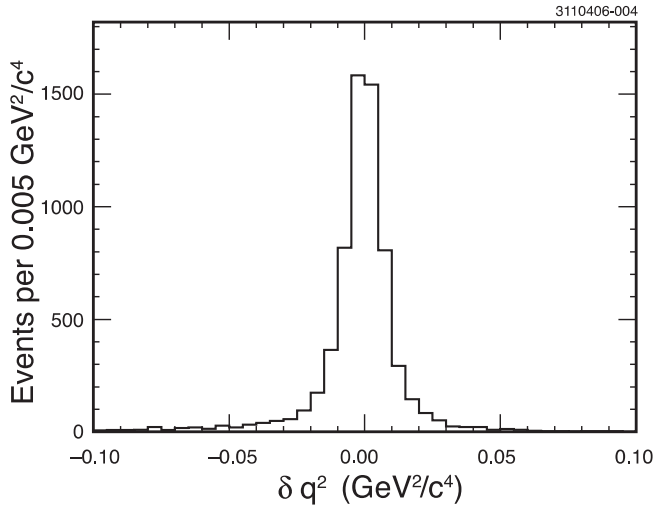

FIG. 3. The q^2 resolution predicted by the generic $D\bar{D}$ MC.

The q^2 resolution predicted by our MC is roughly Gaussian with a root-mean-square (rms) width of $0.02\ \mathrm{GeV}^2/c^4$, which is shown in Fig. 3. This is negligible on the scale in which we will bin our data.

Even though we only measure the shape and not absolute rates, as a cross-check we have measured the $D^+ \to \bar{K}^{*0}e^+\nu_e$ branching fraction assuming an efficiency derived from the generic MC. We found statistical consistency with the result in Ref. [18].

III. PROJECTION WEIGHTING TECHNIQUE

We extract the helicity basis form factors using the projective weighting technique more fully described in Ref. [10]. For a given q^2 bin, a weight is assigned to the event depending on its θ_V and θ_ℓ decay angles. We use 25 joint $\Delta\cos\theta_V \times \Delta\cos\theta_\ell$ angular bins: 5 evenly spaced bins in $\cos\theta_V$ times 5 bins in $\cos\theta_\ell$.

For each q_i^2 bin, the angular distribution can be written as a vector $\vec{N}_i$ whose components give the number of

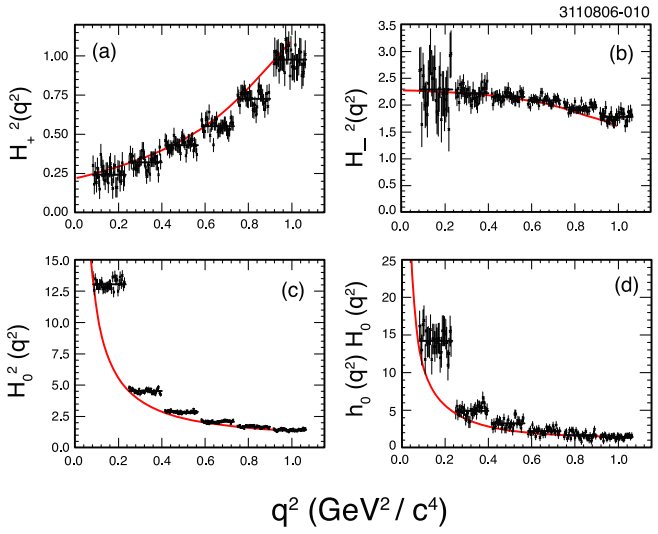

FIG. 4 (color online). Monte Carlo study of the projective weighting technique errors and biases. The reconstructed form factors are the points with error bars. The curves give the helicity form factor products assumed in the simulations. Thirty independent simulations were used for each q^2 bin. The averages of the simulated results are given by the horizontal lines. Their actual ordinate is at the left of the averaging line. The yield in these MC samples are 6 times the yield in the data. The plots are: (a) $H_+^2(q^2)$, (b) $H_-^2(q^2)$, (c) $H_0^2(q^2)$, and (d) $h_0(q^2)H_0(q^2)$.

events reconstructed in each of the 25 angular bins. According to Eq. (1), $\vec{N}_i$ can be written as a linear combination of $\vec{m}_\alpha$ vectors with coefficients $f_\alpha(q_i^2)$,

$$\vec{N}_i = f_+(q_i^2)\vec{m}_+ + f_-(q_i^2)\vec{m}_- + f_0(q_i^2)\vec{m}_0 + f_I(q_i^2)\vec{m}_I. \quad (4)$$

The $\vec{m}_+$, $\vec{m}_-$, $\vec{m}_0$, and $\vec{m}_I$ vectors are computed using a full detector simulation weighted by the corresponding helicity term in Eq. (1). For example, $\vec{m}_+$ is computed using a simulation generated with an arbitrary function for $H_+(q^2)$ (such as $H_+(q^2) = 1$) and zero for the remaining three form factors. The $f_\alpha(q_i^2)$ functions are proportional to the true $H_\alpha^2(q_i^2)$ along with multiplicative factors such as $G_F^2|V_{cs}|^2(q^2 - m_\ell^2)$ and additional corrections accounting for experimental effects such as acceptance.

Reference [10] shows how Eq. (4) can be solved for the four form factor products $H_+^2(q^2)$, $H_-^2(q^2)$, $H_0^2(q^2)$, and $h_0(q^2)H_0(q^2)$ by making four weighted q^2 histograms. The weights are directly constructed from the four $\vec{m}_\alpha$ vectors. We have tested the method using 30 independent Monte Carlo samples. Figure 4 demonstrates that the projective weighting technique returns realistic errors with no significant bias.

IV. RESULTS

Figure 5 shows the four form factor products multiplied by q^2 obtained for data using the nominal selection criteria. In this figure, the background estimated from the generic charm MC simulation is subtracted. For the nominal selection we estimate that 3.6% of the events are background. The form factors are normalized by scaling the four weighted histograms ($H_\pm^2(q^2)$, $H_0^2(q^2)$, and $h_0(q^2)H_0(q^2)$) by a common factor so that $q^2H_0^2(q^2) = 1$ as $q^2 \to 0$.[1] Because of our excellent q^2 resolution, there is negligible correlation among the six q^2 bins for a given form factor product, but the relative correlations between different form factor products in the same q^2 bin can be as high as 36%. The $h_0(q^2)H_0(q^2)$ form factor in Fig. 5(d) is measured through the interference term of Eq. (1), which is proportional to $\mathrm{Re}\{\mathcal{A}e^{-i\delta}BW\}$. Averaging over the full $m_{K\pi}$ mass range, $\mathrm{Re}\{\mathcal{A}e^{-i\delta}BW\}$ is proportional to $-\mathcal{A}\sin\delta$. The interference term is then measured by a fourth projective weight and divided by the FOCUS $-\mathcal{A}\sin\delta$ value [9] to obtain $h_0(q^2)H_0(q^2)$. The measurement on $h_0(q^2)H_0(q^2)$ includes a systematic uncertainty due to uncertainties in $\mathcal{A}\sin\delta$, which we discuss below.

Figure 6 shows the helicity amplitudes without q^2 weighting, thus emphasizing the low q^2 region. It includes results obtained with the nominal selection criteria as well as the more restrictive selection criteria. The background fraction in the tightly selected sample is only 0.4% of the event sample and its background subtraction is negligible.

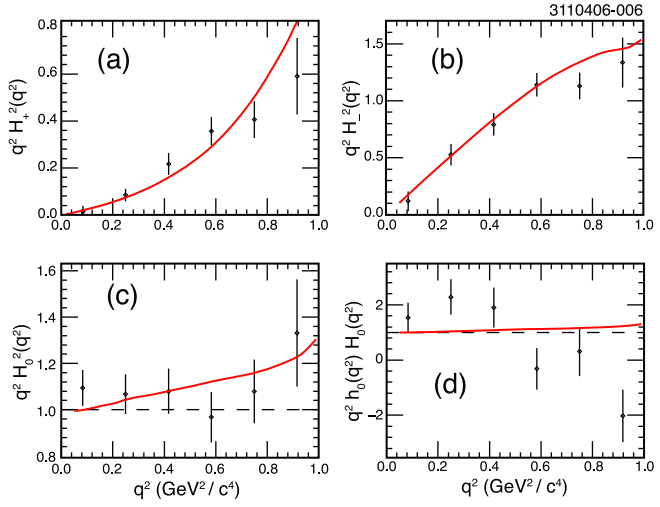

FIG. 5 (color online). Measured form factor products for six q^2 bins. The data are points with error bars representing only the statistical uncertainties. The solid curves are obtained using the form factor representation and the parameters reported in Ref. [9], namely: $V(0)/A_1(0) = 1.505$, $A_2(0)/A_1(0) = 0.875$, and s-wave parameters $\mathcal{A} = 0.33$ and $\delta = 39°$. The histogram plots are: (a) $q^2H_+^2(q^2)$, (b) $q^2H_-^2(q^2)$, (c) $q^2H_0^2(q^2)$, and (d) $q^2h_0(q^2)H_0(q^2)$.

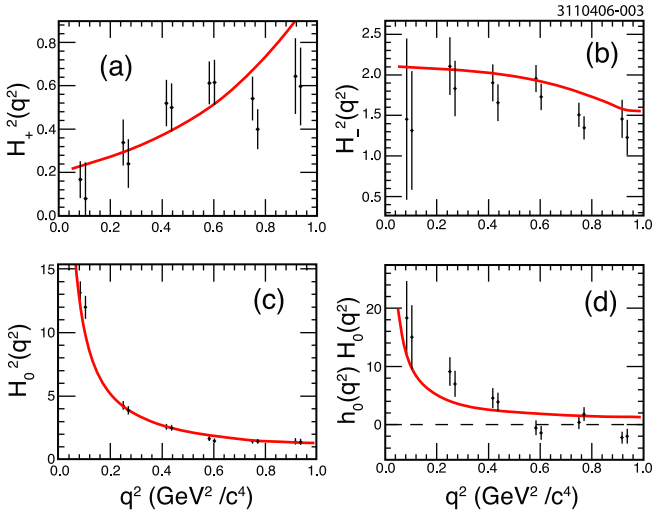

FIG. 6 (color online). Measured form factor products for six q^2 bins. We show the results obtained with the nominal selection criteria (first point in each bin) and the tighter selection criteria (second point in each bin). The error bars represent statistical uncertainties only. The solid curves are obtained using the form factor representation and the parameters reported in Ref. [9]. The histogram plots are: (a) $H_+^2(q^2)$, (b) $H_-^2(q^2)$, (c) $H_0^2(q^2)$, and (d) $h_0(q^2)H_0(q^2)$.

[1]The details of the normalization procedure are as follows: The solid curve in Fig. 5(c) represents the parametrized model for the form factor $q^2H_0^2(q^2)$ presented in Ref. [9]. This curve is normalized to 1 at $q^2 \to 0$. Then our data points in Fig. 5(c) are scaled to the curve by a factor obtained from a χ^2 fit. The data points in the other Fig. 5 histograms are all scaled by the same factor.

TABLE I. Summary of form factor product results for six q^2 bins. Each form factor product is averaged over the indicated q^2 range. The first and second errors are statistical and systematical uncertainties, respectively. The numbers are normalized using the condition: $q^2 H_0^2(q^2) = 1$ as $q^2 \to 0$.

q^2 range (GeV$^2/c^4$)	H_+^2	H_-^2	H_0^2	$h_0 H_0$
0.000 − 0.167	0.16 ± 0.12 ± 0.03	1.19 ± 0.87 ± 0.49	13.17 ± 0.91 ± 0.13	13.60 ± 4.72 ± 1.86
0.167 − 0.334	0.32 ± 0.10 ± 0.02	1.99 ± 0.34 ± 0.16	4.30 ± 0.34 ± 0.04	6.73 ± 1.84 ± 0.92
0.334 − 0.501	0.52 ± 0.11 ± 0.01	1.88 ± 0.23 ± 0.08	2.59 ± 0.23 ± 0.04	3.34 ± 1.25 ± 0.46
0.501 − 0.668	0.61 ± 0.10 ± 0.01	1.93 ± 0.17 ± 0.08	1.69 ± 0.18 ± 0.01	−0.36 ± 0.94 ± 0.08
0.668 − 0.835	0.55 ± 0.10 ± 0.01	1.53 ± 0.15 ± 0.03	1.43 ± 0.18 ± 0.03	0.35 ± 0.87 ± 0.06
0.835 − 1.000	0.65 ± 0.18 ± 0.01	1.46 ± 0.23 ± 0.03	1.47 ± 0.25 ± 0.02	−1.78 ± 0.84 ± 0.24

The consistency of the two results shows that the systematic error due to background subtraction is small.

We have considered several sources of systematic uncertainties. Even though we have very little background in our data set, the background subtraction still constitutes the primary source of systematic error. For this uncertainty, we assign a conservative value by reducing the level of the background being subtracted by a factor of 2 and comparing these form factor products with the results based on the full background subtraction. For $H_+^2(q^2)$, the background systematic uncertainty is estimated to be 16.5% for the first q^2 bin and less than 4.8% for higher bins. For $H_-^2(q^2)$, the background systematic uncertainty is estimated to be 41.3% for the first q^2 bin and less than 8.1% for higher bins. For $H_0^2(q^2)$, the background systematic uncertainty is estimated to be less than 2.1%; and for $h_0 H_0$, the background systematic uncertainty is estimated as less than 18.0%. The systematic uncertainty due to track reconstruction and particle identification is rather low since we are reporting on form factor shapes rather than absolute normalization. The systematic uncertainty from these sources is estimated as less than 1.9% for all of the form factor products. Lastly, we assess an additional scale error of 13.4% for the $h_0 H_0$ form factor product due to the uncertainties in the $\mathcal{A}$ and δ values reported in Ref. [9]. Our total systematic uncertainty is the quadrature sum of these systematic contributions and found to be small compared to the statistical uncertainty. In all cases except $h_0 H_0$, the systematic uncertainty is dominated by the background systematic uncertainty. Table I gives the q^2 range for each bin, along with the form factor products, their statistical uncertainty (first error), and the estimated systematic uncertainty (second error).

Figures 5(d) and 6(d) show that the $h_0(q^2)H_0(q^2)$ form factor product is in rough agreement with the model from Ref. [9]. We are also consistent with the FOCUS s-wave phase $\delta = 39 \pm 5°$. Our consistency check is the comparison of the s-wave interference term for events with $m_{K\pi}$ below and above the $\bar{K}^{*0}$ pole as shown in Fig. 7. The interference between the s-wave and the Breit-Wigner is proportional to $\cos(\delta - \beta_\pm)$ where β_- and β_+ are the average Breit-Wigner phases below and above the $\bar{K}^{*0}$ pole, respectively. In the mass region where $m(\bar{K}^{*0}) < m_{K\pi} < 1.0$ GeV, β_+ is $-59°$, which is nearly orthogonal to the FOCUS s-wave phase. If our phase is consistent with the FOCUS phase, the effective $h_0(q^2)H_0(q^2) \times \mathrm{Re}\{\mathcal{A}e^{-i\delta}\langle BW\rangle\}$ should disappear above the $\bar{K}^{*0}$ pole as it does in Fig. 7(b). The sum of the first three bins of the histogram of Fig. 7(a) differs from zero by 5.9 standard deviations. This confirms the earlier observation [8] of an s-wave interference with the FOCUS phase, but does not provide an independent measurement of that phase.

It is of interest to search for the possible existence of additional nonresonant amplitudes of higher angular momentum. It is fairly simple to extend Eq. (1) to account for potential d-wave or f-wave interference with the $\bar{K}^{*0}$ Breit-Wigner. We search specifically for a possible zero helicity d-wave or f-wave piece that interferes with the zero helicity $\bar{K}^{*0}$ contribution. One expects that potential $h_0^{(d)}(q^2)$ and $h_0^{(f)}(q^2)$ form factors would peak as $1/\sqrt{q^2}$ near $q^2 \to 0$ as is the case for the other zero helicity contributions $H_0(q^2)$ and $h_0(q^2)$. If so, the zero helicity contributions should be much larger than potential d- or f-wave ± 1 helicity contributions. The d- and f-wave interference terms are the same as the s-wave interference term apart from additional Wigner d-matrices. These describe anisotropy in the d- and f-wave decays. The additional factors are $d_{0,0}^2(\theta_V)$ for the d-wave and

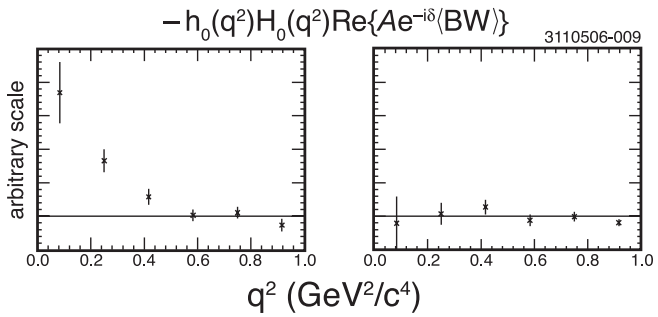

FIG. 7. The s-wave interference term for the events (a) below the $\bar{K}^{*0}$ pole and (b) above the pole. The interference term depends on the s-wave phase relative to the average phase of the Breit-Wigner in the corresponding plot. All of the $\cos\theta_V$ interference observed by FOCUS [8] was also below the $\bar{K}^{*0}$ pole.

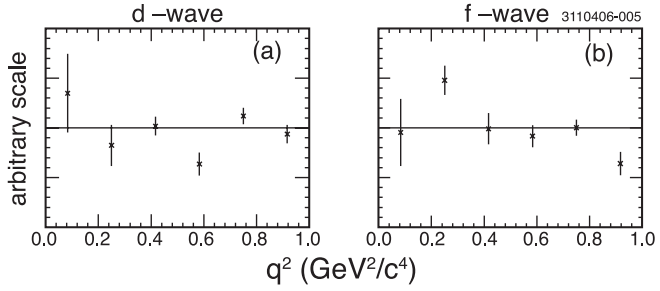

FIG. 8. Search for (a) d-wave and (b) f-wave interference effects, $\mathcal{A}_{d,f}\sin\delta_{d,f}h_0^{(d,f)}(q^2)H_0(q^2)$, as described in the text.

$d^3_{0,0}(\theta_V)$ for the f-wave. Hence, the d-wave weights are based on a fifth term of the form $4\sin^2\theta_\ell\cos\theta_V(3\cos^2\theta_V - 1)H_0(q^2)h_0^{(d)}(q^2)\,\mathrm{Re}\{\mathcal{A}_d e^{-i\delta_d}BW\}$ in Eq. (1). The f-wave weights are based on a fifth term of the form $4\sin^2\theta_\ell\cos\theta_V(5\cos^3\theta_V - 3\cos\theta_V)H_0(q^2)h_0^{(f)}(q^2)\times \mathrm{Re}\{\mathcal{A}_f e^{-i\delta_f}BW\}$. Averaging over the Breit-Wigner, the interference should be proportional to $\mathcal{A}_{d,f}\sin\delta_{d,f}h_0^{(d,f)}(q^2)H_0(q^2)$.

Figure 8 shows the $\mathcal{A}_{d,f}\sin\delta_{d,f}h_0^{(d,f)}(q^2)H_0(q^2)$ obtained with this technique. It is apparent from Fig. 8 that we have no compelling evidence for either a d-wave or an f-wave component. Unfortunately, we cannot set a particularly stringent limit. Under the assumption $h_0^{(d,f)}(q^2) = H_0(q^2)$, used in Ref. [9], we perform a χ^2 fit of Fig. 8 to the form $\mathcal{A}_{d,f}\sin\delta_{d,f}H_0^2(q^2)$. The results of these fits were $\mathcal{A}_d\sin\delta_d = -0.07 \pm 0.20$ and $\mathcal{A}_f\sin\delta_f = 0.17 \pm 0.18$. For comparison, the value for $\mathcal{A}\sin\delta$ for the s-wave contribution according to Ref. [9] is 0.21 ± 0.028.

V. SUMMARY

We present a nonparametric analysis of the helicity basis form factors that control the kinematics of the $D^+ \to K^-\pi^+e^+\nu_e$ decays. We use a projective weighting technique that allows one to determine the helicity form factor products by weighted histograms rather than likelihood based fits. The resulting helicity form factors have very little background and the background subtraction procedure is well understood. We confirm the existence of an s-wave $K^-\pi^+$ component to the $D^+ \to K^-\pi^+e^+\nu_e$ decay and have studied the q^2 dependence of its form factor. Finally, we have searched for possible d-wave or f-wave nonresonant interference contributions to $D^+ \to K^-\pi^+e^+\nu_e$. Although we have no statistically significant evidence for f-wave or d-wave interference, we are unable to limit these terms to appreciably less than the established s-wave interference.

ACKNOWLEDGMENTS

We gratefully acknowledge the effort of the CESR staff in providing us with excellent luminosity and running conditions. D. Cronin-Hennessy and A. Ryd thank the A. P. Sloan Foundation. This work was supported by the National Science Foundation, the U.S. Department of Energy, and the Natural Sciences and Engineering Research Council of Canada.

[1] S. Bianco, F. L. Fabbri, D. Benson, and I. Bigi, Riv. Nuovo Cimento **26N7**, 1 (2003).

[2] M. Bauer, B. Stech, and M. Wirbel, Z. Phys. C **29**, 637 (1985); M. Bauer and M. Wirbel, Z. Phys. C **42**, 671 (1989); J. G. Korner and G. A. Schuler, Z. Phys. C **46**, 93 (1990); F. J. Gilman and R. L. Singleton, Phys. Rev. D **41**, 142 (1990); D. Scora and N. Isgur, Phys. Rev. D **52**, 2783 (1995); B. Stech, Z. Phys. C **75**, 245 (1997); D. Melikhov and B. Stech, Phys. Rev. D **62**, 014006 (2000).

[3] P. Ball, V. M. Braun, H. G. Dosch, and M. Neubert, Phys. Lett. B **259**, 481 (1991); P. Ball, V. M. Braun, and H. G. Dosch, Phys. Rev. D **44**, 3567 (1991).

[4] C. W. Bernard, A. X. El-Khadra, and A. Soni, Phys. Rev. D **45**, 869 (1992); V. Lubicz, G. Martinelli, M. S. McCarthy, and C. T. Sachrajda, Phys. Lett. B **274**, 415 (1992); A. Abada *et al.*, Nucl. Phys. **B416**, 675 (1994); K. C. Bowler *et al.* (UKQCD Collaboration), Phys. Rev. D **51**, 4905 (1995); T. Bhattacharya and R. Gupta, Nucl. Phys. B, Proc. Suppl. **47**, 481 (1996); C. R. Alton *et al.* (APE Collaboration), Phys. Lett. B **345**, 513 (1995); S. Gusken, G. Siegert, and K. Schilling, Prog. Theor. Phys. Suppl. **122**, 129 (1996); A. Abada *et al.* (SPQcdR Collaboration), Nucl. Phys. B, Proc. Suppl. **119**, 625 (2003).

[5] S. Fajfer and J. Kamenik, Phys. Rev. D **72**, 034029 (2005).

[6] G. S. Huang *et al.* (CLEO Collaboration), Phys. Rev. Lett. **95**, 181801 (2005); M. Ablikim *et al.* (BES Collaboration), Phys. Lett. B **608**, 24 (2005); J. M. Link *et al.* (FOCUS Collaboration), Phys. Lett. B **598**, 33 (2004).

[7] J. M. Link *et al.* (FOCUS Collaboration), Phys. Lett. B **544**, 89 (2002); M. Adamovich *et al.* (BEATRICE Collaboration), Eur. Phys. J. C **6**, 35 (1999); E. M. Aitala *et al.* (E791 Collaboration), Phys. Rev. Lett. **80**, 1393 (1998); Phys. Lett. B **440**, 435 (1998); P. L. Frabetti *et al.* (E687 Collaboration), Phys. Lett. B **307**, 262 (1993); K. Kodama *et al.* (E653 Collaboration), Phys. Lett. B **274**, 246 (1992); J. C. Anjos *et al.* (E691 Collaboration), Phys. Rev. Lett. **65**, 2630 (1990).

[8] J. M. Link *et al.* (FOCUS Collaboration), Phys. Lett. B **535**, 43 (2002).

[9] J. M. Link *et al.* (FOCUS Collaboration), Phys. Lett. B **544**, 89 (2002).
[10] J. M. Link *et al.* (FOCUS Collaboration), Phys. Lett. B **633**, 183 (2006).
[11] J. G. Korner and G. A. Schuler, Z. Phys. C **46**, 93 (1990).
[12] Y. Kubota *et al.* (CLEO Collaboration), Nucl. Instrum. Methods Phys. Res., Sect. A **320**, 66 (1992); M. Artuso *et al.*, Nucl. Instrum. Methods Phys. Res., Sect. A **554**, 147 (2005); D. Peterson *et al.*, Nucl. Instrum. Methods Phys. Res., Sect. A **478**, 142 (2002).
[13] Q. He *et al.* (CLEO Collaboration), Phys. Rev. Lett. **95**, 121801 (2005).
[14] D. J. Lange, Nucl. Instrum. Methods Phys. Res., Sect. A **462**, 152 (2001).
[15] R. Brun *et al.*, CERN Program Library Long Writeup, Report No. W5013 (unpublished).
[16] E. Barberio, B. van Eijk, and Z. Wąs, Comput. Phys. Commun. **66**, 115 (1991); E. Barberio and Z. Wąs, Comput. Phys. Commun. **79**, 291 (1994).
[17] S. Eidelman *et al.*, Phys. Lett. B **592**, 1 (2004).
[18] G. S. Huang *et al.* (CLEO Collaboration), Phys. Rev. Lett. **95**, 181801 (2005).